

EXPERIMENTATION AND PHYSICS AT A FUTURE ELECTRON-POSITRON LINEAR COLLIDER

MARTIN POHL

DPNC, Université de Genève, Switzerland

and

EHEF, Katholieke Universiteit Nijmegen, The Netherlands

E-mail: Martin.Pohl@cern.ch

I summarise the physics opportunities and experimental challenges at future Linear Colliders, using material from the recent ECFA/DESY workshop on the subject as well as contributions to the series of worldwide studies. For reasons of economy, the discussion is restricted to the European Tesla project and to its electron-positron mode only.

1 Yet Another Accelerator?

Experimentation at the current generation of high energy colliders, LEP at CERN and the Tevatron at FNAL, is not yet completed. The next generation hadron collider LHC at CERN is on track but far from finished. One may thus wonder why now is the right time to discuss future accelerator projects. The reason is that the recent past shows that a new generation of accelerators takes of order 10 years to prepare. It takes another ~ 10 years to build and commission the machine and its experiments. Consequently, the preparations for a successor to LEP started in the early 1990. And it is now the time to design the next lepton machine and its integrated experiments – and get them approved – to answer the physics questions of 2010.

It is obvious to everyone that the current generation of machines and experiments surpassed expectations by a large margin. LEP and SLC established the electroweak sector of the Standard Model at the loop level, with such precision that even the mass of inaccessible particles is predicted from radiative corrections with respectable precision¹. The Tevatron experiments discovered the top quark at the mass required for radiative corrections and thus completed the periodic system of matter required by the Standard Model. Nevertheless, as good an effective theory as the Standard Model may be, it still remains an effective theory with many unanswered questions. We list only a few:

- Current data do not exclude the existence of a Higgs boson, provided

¹Invited talk given at the XXVIII International Meeting on Fundamental Physics, Sanlúcar de Barrameda, Cádiz, Spain, 14-18 February 2000

that it is rather light. But we still miss experimental evidence for this mechanism of mass generation proposed by the Standard Model.

- Gravity is completely missing from the current picture based on gauge theories.
- A rationale for the values of couplings and their potential unification is not provided by the Standard Model. In particular the structure and values of the CKM^{2,3} and MNS⁴ matrix elements remain a complete mystery.
- The number and hierarchy of fermion generations remains unexplained.
- It is not known why matter apparently consists of fermions only and why forces are transmitted by vector bosons. Supersymmetry proposes to lift this asymmetry.

LHC will clearly greatly contribute to approaching answers to these questions. If a light Higgs particle exists, it will be discovered at LHC. If it does not exist, LHC might reveal interactions among electroweak gauge bosons, resonances at the TeV scale or other mechanisms to cut off electroweak divergences. Structures of space-time responsible for gravitation might be discovered. And last but not least, a large part of the rich spectrum of supersymmetric particles will be observed at LHC if nature chooses to be supersymmetric. Physics after LHC will thus be less focused on the discovery of new physics but on its proper understanding. One can foresee that this effort will focus on three main themes:

- refined knowledge of model parameters, especially the properties of the top quark and the W boson as well as those of supersymmetric particles;
- studies of the Higgs boson – if it exists – to establish the Higgs-like nature of the particle, to measure its couplings to matter and its self-coupling and to distinguish between the standard Higgs and its supersymmetric alternatives;
- understanding of alternative mechanisms – if the Higgs mechanism is not realised – in the study of new states in boson scattering or in the search for a substructure of matter.

In a sense, LHC will thus point out the way towards a new effective theory replacing the Standard Model. And a second generation machine will be required to establish this new effective theory, much in the way that LEP

established the Standard Model itself. I believe that such a machine should be an electron-positron collider. While not so much fit for exploratory studies into a completely unknown energy domain, their fixed beam energy, fully available for annihilation reactions and providing constrained final state kinematics, make them ideal machines for dedicated studies in well defined energy ranges.

Electron-positron cross sections in the interesting energy range, from top threshold to 1 TeV, are much smaller than cross sections at LEP. One thus needs a machine that exceeds current e^+e^- collider luminosities by two orders of magnitude. Synchrotron radiation power losses prevent us from extrapolating the successful technology of circular electron-positron colliders to higher energies. The power loss, P_B , on a circular orbit of radius R is proportional to

$$P_B \sim \frac{E_b^3}{m^3 R} \quad (1)$$

with the particle energy E and its mass m . LEP, with a circumference of 27 km, will thus be the largest circular e^+e^- collider ever to be built. There are two ways to efficiently fight radiation energy loss in a lepton collider. One is to use heavier leptons as is done in muon collider projects⁵. The other one is to take the radius to infinity, which is the idea behind Linear Colliders, pioneered with the SLC. In addition, Linear Colliders feature potentially high beam polarisation, crucial for the measurement of spin dependent amplitudes and the suppression of background. I thus believe that a Linear electron-positron Collider is the right choice for a first generation machine directly after LHC.

This report is based on material from the *Second Joint ECFA/DESY Study on Physics and Detectors for a Linear Electron-Positron Collider*⁶ as well as the *Worldwide Study on the Physics and Detectors for Future Linear e^+e^- Colliders*⁷. Most of the material comes from the Tesla Conceptual Design Report^{8,9} (CDR), the Sitges workshop of the worldwide study¹⁰ and the Obernai workshop of the ECFA/DESY study¹¹.

2 The Tesla Machine

The figures of merit that characterise any machine for the experimenter are the center of mass energy, \sqrt{s} , and the luminosity, \mathcal{L} . Superconducting Linear Colliders present advantages over normal conducting ones. I will concentrate on only two aspects: the high power conversion efficiency and the comparatively relaxed alignment tolerances.

The luminosity of a collider can be written as¹⁴

$$\mathcal{L} = \frac{n_b N_e^2 f}{4\pi\sigma_x\sigma_y} H_D \quad (2)$$

where n_b is the number of bunches/pulse, N_e the number of e^\pm per bunch, f the pulse repetition frequency and $\sigma_{x,y,z}$ are the horizontal, vertical and longitudinal beam sizes at the interaction point. The disruption enhancement factor, H_D , is due to the pinch effect that focuses one bunch in the field of the other; it has typical values of $\simeq 1.5$.

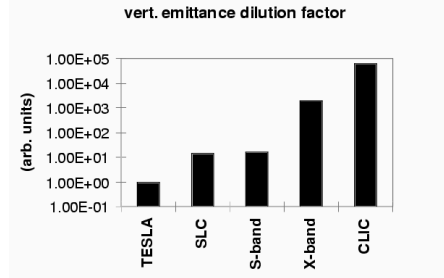


Figure 1. Comparison of the expected vertical emittance dilution factor F for the Tesla low frequency, superconducting Linear Collider compared to high frequency normal conducting ones.

The luminosity can also be given in terms of the average beam power, P_b , at a given center of mass energy, \sqrt{s} ,

$$P_b = n_b N_e f \sqrt{s} = \eta P_{AC} \quad (3)$$

which is the product of the AC power consumption, P_{AC} , and the power conversion efficiency, η . This efficiency can be as high as 16% for a superconducting Linear Collider, which is the first of the major advantages of this technology. The remaining parameters of the luminosity can be expressed in terms of the fraction, δ_E , of beam energy lost by collective beamstrahlung

$$\delta_E = \frac{\Delta E_b}{E_b} \sim \frac{r_e^3 N_e \gamma}{\sigma_z (\sigma_x + \sigma_y)^2} \sim \frac{r_e^3 N_e \gamma}{\sigma_z \sigma_x^2} \quad (4)$$

The rightmost proportionality is reached in the limit of flat beams $\sigma_x \gg \sigma_y$, which allows to maximise luminosity without intolerable beamstrahlung losses by reducing the vertical beam size σ_y . The beam phase space at the interaction point is given by the emittance, ϵ , and the β function

$$\sigma_y = \sqrt{\epsilon_y \beta_y} \quad (5)$$

where a $\beta_y \simeq \sigma_z$ corresponds to a practical limit. The luminosity in these terms thus becomes

$$\mathcal{L} \sim \frac{\eta P_{AC}}{\sqrt{s}} \sqrt{\frac{\delta_E}{\epsilon_y}} H_D \quad (6)$$

inversely proportional to the square root of the emittance. The second major advantage of superconducting technology is that it allows for low emittance dilution by short range wake fields. This dilution depends on the r.m.s. lattice misalignment, δy^2 ,

$$\frac{\Delta\epsilon}{\epsilon} \sim F \bar{\beta} \delta y^2 \quad (7)$$

with a dilution factor, F , which is extremely dependent on the radiofrequency, f_{RF} ,

$$F \sim \frac{N_e^2 \sigma_z f_{RF}^6}{\epsilon_y} \quad (8)$$

Fig. 1 shows a comparison between the expected dilution factors for the vertical emittance of Tesla as compared to high frequency normal conducting machines which are under study in Japan¹³ and in the USA¹² and which aim at similar performance. A low frequency, typical for superconducting accelerators, is thus very beneficial in that it reduces the requirements for alignment tolerances, yet preserving high luminosity.

It is unrealistic to expect that accelerating gradients in a superconducting cavity were to rise above some 40 MV/m. Surface defects that even the most careful conditioning cannot prevent, limit realistic gradients to such values. It is therefore clear that a superconducting Linear Collider like Tesla will not enter into the TeV energy domain. Beyond that frontier, novel accelerating techniques like the two-beam accelerator CLIC will have to come into play. However, a machine with up to 1 TeV energy indeed covers most of the LHC's discovery range and is thus entirely appropriate as a first generation machine for the era after LHC.

I will limit further discussions to the proposed Tesla machine. Fig. 2 shows the layout of the machine complex. Its major parameters are summarised in Tab. 1 and compared to the performance of LEP. Mind that the contents of this table is my own interpretation of numbers from various sources and not an official Tesla design specification. It clearly includes some amount of wishful thinking of an experimenter *in spe*.

One of the major challenges in reaching these ambitious goals is the accelerating gradient in excess of 25 MV/m required to keep the tunnel length

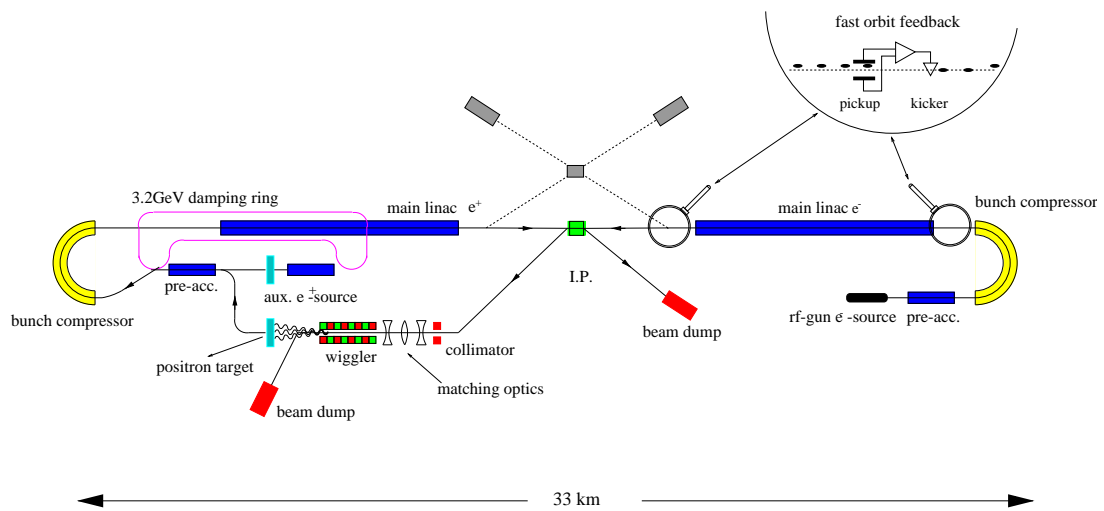


Figure 2. Layout of the Tesla machine complex (not to scale) showing the principle machine components.

Table 1. Comparison of machine performance parameters between what has actually been achieved at LEP 200 and what the eager experimenter might hope for at Tesla. This is not a compilation of official Tesla design goals.

	LEP 200	TESLA	
type	Storage Ring	Linear Collider	
maximum energy	200 GeV	500 GeV	800 GeV
total length	26.7 km	33km	
accelerating gradient	6 MV/m	25 MV/m	40 MV/m
maximum bunches	8	1410	4028
beam size at IP [μm]	150×10	0.85×0.02	0.34×0.02
luminosity [$\text{cm}^{-2}\text{s}^{-1}$]	10^{32}	1×10^{34}	5×10^{34}

inside reasonable limits. Fig. 3 shows a nine-cell niobium superconducting cavity of which Tesla will need about twenty thousand. These are now produced by several European companies and tested at the DESY Tesla Test Facility. In recent production, both the quality factor and the maximum gradient have consistently exceeded the requirements. As an example, Fig. 3 shows the statistics of accelerating gradients. The more experience in production and post-production conditioning is gained, the more cavities exceed the required minimum gradients.

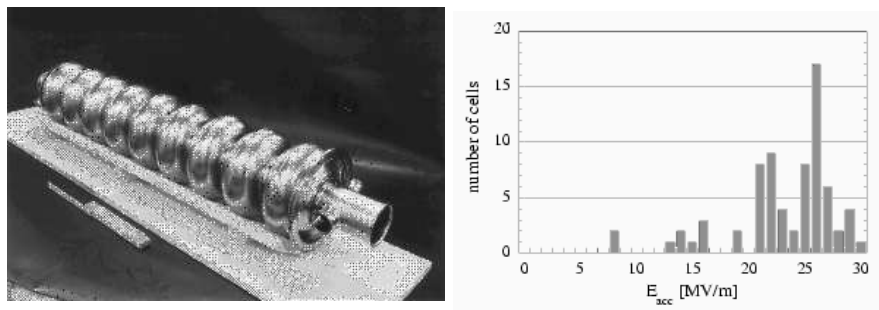


Figure 3. Left: Nine cell niobium cavity for Tesla. Right: Statistics of accelerating gradients in early cavity production. Performance exceeding specifications are routinely reached by industry after a short learning phase.

Another challenge is in the final focus, required to produce the tiny beam sizes at the interaction point. Final focus test facilities are available at SLAC and DESY. The beam delivery system with collimation, tuning section and final transformer will be several kilometers long, a substantial fraction of the total collider length. The final transformer will demagnify the beam by a

factor of 15 in the vertical and 50 in the horizontal plane. Such large focusing forces inevitably create a large amount of synchrotron radiation close to the interaction point which have to be shielded by a sophisticated system of masks. Their unshieldable component as well as the closest mask has to be accommodated by a forward-backward hole in the detector (see Fig. 5).

The whole Tesla complex will be housed in a single 5m diameter tunnel, with minimal environmental impact, including the main linac and the damping ring as well as all services.

3 A Tesla Detector

As will be shown below, physics at a Linear Collider requires a detector with truly excellent performance. Physics requirements focus on three main aspects:

- *Hadronic jets*: an excellent resolution for charged particles as well as high granularity calorimetry are required to obtain the necessary resolution on jet energy and direction as well as jet-jet mass. Identification of bottom and charm jets is a must, thus excellent vertexing is required.
- *Leptons*: electron-hadron distinction requires excellent tracking resolution as well as electromagnetic energy resolution. Again, fine grain calorimetry must allow to tag electrons close to a jet. Obviously, muon identification is a must.
- *Missing energy and momentum*: In order to take advantage of the constrained final state kinematics, one needs redundancy in the tracker and calorimeter subsystems. The energy flow methodology must be used to fully take advantage of this redundancy. The detector has to be hermetic down to the mask shielding synchrotron radiation.

A conservative model detector that fulfils these basic requirements has been described in the Tesla Conceptual Design Report⁸. Its layout is shown in Fig. 4. I will summarise its main design features in the following. I will also point out less conservative alternatives for subsystems that are being discussed presently.

It is tempting to scale one of the LEP detectors to obtain a viable model for a Linear Collider detector at energies two to four times higher. And indeed the detector described in the Tesla CDR conceptually resembles the Aleph detector rather closely. Nevertheless, the smaller beam pipe allows for instrumentation down to smaller radius, with finer grain detectors of higher

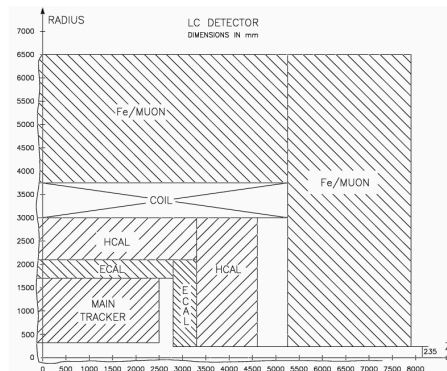


Figure 4. Sketch of the Tesla detector layout as described in the TDR.

resolution, as pioneered by SLD. Although the average particle energy varies little with the center of mass energies in hadron production, the maximum momenta in low multiplicity leptonic final states are of the order of the beam energy. Thus, better point resolutions, more measured points on the trajectory and higher magnetic fields are required for the tracking device. And the higher maximum electron, photon and hadron energies point towards thicker electromagnetic and hadronic calorimeters. The subdetectors of the Tesla detector study have been dimensioned accordingly, as shown in Fig. 4.

The inner detector, with the tracker and the full calorimeters, is enclosed in a superconducting solenoidal magnet of 6m inner diameter and more than 10m length. The CDR study foresaw 3T field strength, with a total stored energy of 1300 MJ. Since then, studies for LHC magnets – like the CMS¹⁵ one – have shown that higher stored energies are feasible. Optimisation towards a 4T magnet, storing 2500 MJ, is thus in progress. This will have implications on the machine itself, and influence experimental conditions like the number of spiralling tracks, tracker occupancy and resolution. The magnet is surrounded by an almost 3m thick iron yoke of about 70% filling factor. The remaining 30% of the volume consist of instrumentation for muon detection. A simple large surface detector, like resistive plate chambers¹⁶ arranged in multiple layers, will suffice to provide optimum protection against hadron misidentification.

As has been demonstrated at SLC, Linear Collider beam pipes at the interaction point can have a radius as small as 2cm, thus leading to a first layer of tracking detector at about 2.5cm from the beam. The use of strip

detectors at such a small radius is excluded because of track overlap: a fraction of overlapping hits of order thirty percent would result for realistic strip lengths. Thus, pixel detectors¹⁷ are a must. At around $500\mu\text{m}$ double hit resolution, they suffer no more than 5% of overlapping hits. Fig. 5 shows a possible layout consisting of three cylindrical layers with cone shaped end caps for the outer layers. At small angle, disk shaped forward layers complete the set-up. As far as the sensor itself is concerned, the CCD¹⁸ technology pioneered at SLD is clearly a prime candidate. Alternatively, active pixel detectors are very interesting. Beyond the bump-bonded technology used by e.g. Delphi¹⁹, monolithic active pixel sensors²⁰ are most promising.

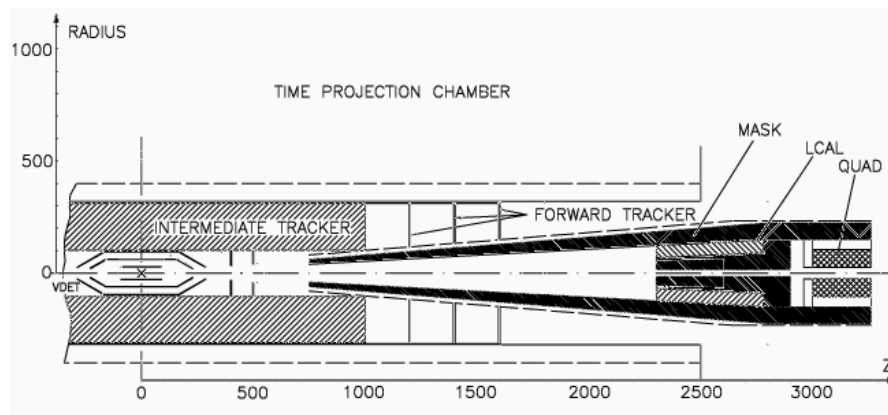


Figure 5. Layout of a pixel vertex detector surrounding the interaction point, supplemented by forward disks surrounding the mask.

For the main tracker, there is hardly any serious alternative to a Time Projection Chamber (TPC)^{21,22}, since no other detector features such a high density of three-dimensional hits with good resolution. In addition, a TPC provides dE/dx measurements for particle identification. Octagonal and circular cross sections are under study. Innovative improvements to cluster detection at the end plates, using the GEM²³ device, are under development. With its large radius, the projected Tesla TPC, together with the vertex detector, would reach a superb momentum resolution as shown in Fig. 6.

Likewise the vertex detector would outperform currently available detectors in an impressive way. Impact parameter resolutions as shown in Fig. 7 are expected, with constant terms of order $5\mu\text{m}$ and multiple scattering terms of order $30\mu\text{m}/p$ (with p in GeV) for the example of the CCD option. Such

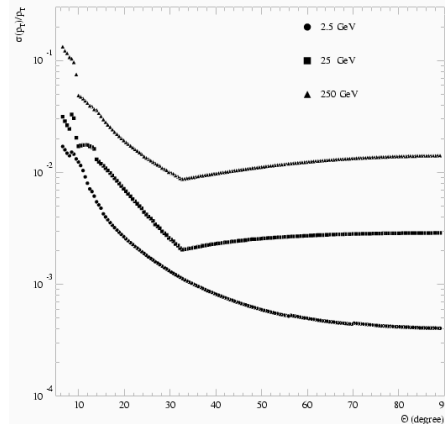


Figure 6. Resolution in the transverse momentum p_t as a function of angle for the Tesla tracking detector at three representative momenta.

performances are indeed required for the measurement of the Higgs Yukawa couplings as shown in Sect. 6.

The Tesla CDR proposes a conservative fine grain calorimeter of “shashlik” readout, inspired by similar DELPHI²⁴ and H1²⁵ calorimeters. In this scheme, a metal/scintillator sandwich is read out radially by wave length shifting fibers crossing absorber plates. The Tesla baseline calorimeter has a physical tower structure. The towers have a granularity of $1^\circ \times 1^\circ$ in the electromagnetic section, where the absorber is lead and the longitudinal sampling is fine. In the hadronic section, made of copper and scintillator, the towers are $2^\circ \times 2^\circ$ wide and the sampling is coarser. All towers almost point to the interaction point, with a small angular deviation to avoid radial cracks in the acceptance. The Tesla CDR quoted rather optimistic performance projections, with a resolution for electromagnetic showers of order $\sigma/E \simeq 0.10/\sqrt{E} \oplus 0.01$ and jet energy resolutions of $\sigma/E \simeq 0.57/\sqrt{E} \oplus 0.01$ (with E in GeV). These estimates need to be substantiated by further simulation studies including more detail on dead material.

Large shashlik type calorimeters are difficult to build since transverse forces tend to stress or even shear off the readout fibers. Therefore, and to optimise space and resolution, other readout schemes, like the tile calorimeter²⁶ with transverse readout are under study. Also radically different and interesting approaches like a silicon-tungsten sampling calorimeter are envisaged

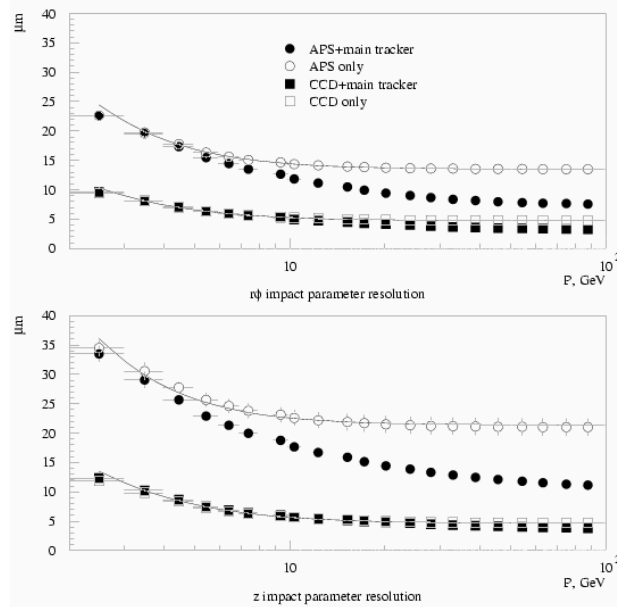


Figure 7. Resolution in the transverse and longitudinal impact parameter for the projected Tesla main tracker and two representative vertex detector performances.

for the electromagnetic section. This technology has so far been restricted to small luminometers^{27,28} but larger scale applications have very attractive features^{29,30} indeed: the resolution is excellent, very fine granularity can be realised in a three-dimensional readout and the set-up is extremely compact. With these technologies, simpler octagonal physical structures can be designed, with towers implemented only in readout.

It is of course not only the subdetector performance that determines performance for physics, but also how they work together, complement each other and create synergy. Tracker and calorimeter measurements of charged particle momentum and energy have to be combined to provide optimum resolution from low to high momenta. Neutral electromagnetic and hadronic energy deposits have to be identified in the calorimeters and separated off charged energy to avoid double counting. The energy flow approach³¹ provides an optimum framework to do this. There, tracker and calorimeter information is combined to provide a system's resolution that is better than the subdetector performance as demonstrated in Fig. 8.

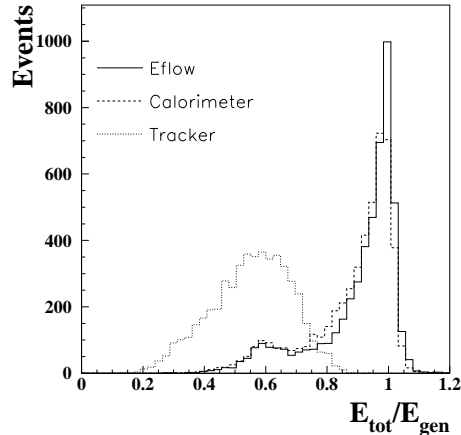


Figure 8. Resolution for the total event energy in hadronic events at 800 GeV as determined from energy flow measurement (solid line), as compared to calorimetric measurements only (dashed line) and charged track momenta only (dotted line).

4 Top Physics

A precision measurement of the top quark mass, m_t , is required to overdetermine electroweak parameters. The most promising method to reach sub-GeV accuracy is to determine the position of the top production threshold³². Unlike the lighter quarks, the top quark decays too quickly to form vector meson resonances in $e^+e^- \rightarrow t\bar{t}$ below threshold. As a consequence, there is hardly an enhancement at threshold as shown in Fig. 9. Moreover, individual initial state radiation (ISR) and collective beamstrahlung effects further wash out the threshold. Strong final state interaction effects cause a dependence of the cross section at threshold on α_s . Measuring an additional observable, however, like the top momentum in addition to the cross section, allows to determine both m_t and α_s simultaneously.

Top production is rather easily identified by requiring one top quark to decay leptonically, $t \rightarrow Wq \rightarrow l\nu q$. The momentum of the top quark can be determined from the other top quark that in general decays hadronically into three jets, $t \rightarrow Wq \rightarrow qq\bar{q}$.

A simulated threshold scan has been evaluated³², with nine points equally spaced in energy, covering $356 < \sqrt{s} < 364$ GeV with a luminosity of 5 fb^{-1}

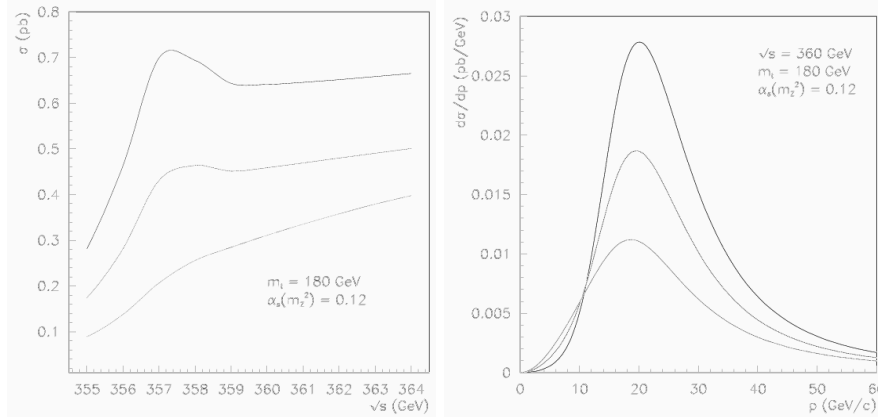


Figure 9. Top production cross section (left) and momentum distribution (right) at Born level (solid line), with initial state radiation (dashed line) and with beamstrahlung (dotted line).

per point. Using both the cross section measurement and the top momentum distribution, one determines the top mass with an accuracy of about 200 MeV, as shown in Fig. 10. This will improve the mass accuracy by a factor of ten with respect to LHC expectations.

Since the width of the loosely bound $t\bar{t}$ systems at threshold is large, interference between S and P states occurs and leads to a forward-backward asymmetry in top production at threshold. While this asymmetry is rather insensitive to both m_t and α_s , it gives an additional handle on the top width. Fig. 10 shows that the top width can thus be determined to an accuracy of about 20%, using all observables from the threshold scan.

Continuum top production at the Linear Collider will allow all the usual measurements of quark properties that have come from e^+e^- machines for the lighter quarks. The coupling of the top quark to the photon will tell about its static electromagnetic properties and reveal an eventual form factor if it has substructure. Likewise, its couplings to the Z will be measured. Its decay properties will determine the $Wt\bar{b}$ coupling. And, maybe most importantly, its coupling to the Higgs boson will be measured, by observing Higgs decay into $t\bar{t}$ if kinematically allowed, by virtual effects otherwise.

Experimental signatures of top quark production include very high particle multiplicities, multi-jet and multi-lepton final states. Their efficient detection requires a high resolution, fine granularity detector.

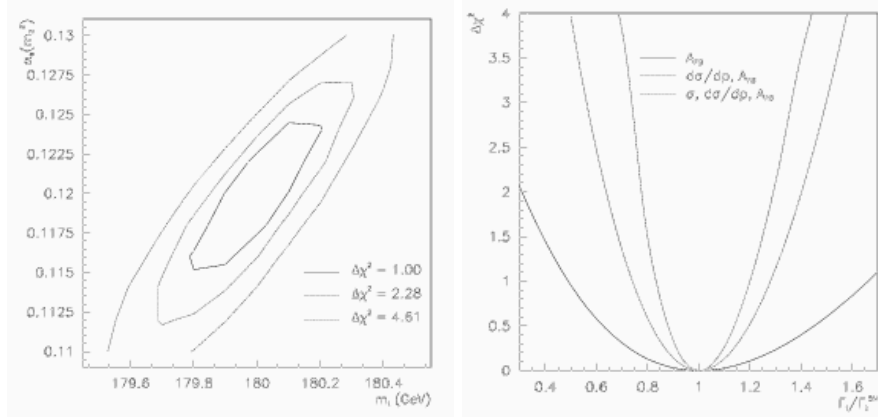


Figure 10. Left: Simultaneous determination of m_t and α_s in a threshold scan. Right: Determination of the top width using the cross section, momentum distribution and forward-backward asymmetry.

5 Weak Boson Physics

The Higgs mechanism relates the masses of the weak bosons to their couplings in standard electroweak theory. At Born level one has

$$\sin^2 \theta_W = 1 - M_W^2/M_Z^2 \quad (9)$$

where θ_W is the weak mixing angle defined by the ratio of weak charged and neutral current couplings. Precision measurements of the couplings at LEP¹ or in neutrino experiments³³ can thus be expressed in terms of the W mass. The comparison with direct measurements of the W mass at LEP and hadron colliders¹ provides one of the stringent tests of electroweak unification and the consistency of the Standard Model.

The measurement of the Z boson mass is not likely to be improved over the precision reached at LEP in the foreseeable future. Even a dedicated run of Tesla at the Z pole³⁴, providing 10^9 Z events with polarised electrons and maybe also positrons will not improve on the mass precision which is limited by systematics. However, one may expect that the measurement of $\sin^2 \bar{\theta}_W$, the effective electroweak mixing angle, would improve by a factor of ten³⁵. The W mass measurement will also improve over current errors, which are expected to reach 30 MeV at the end of LEP-200. LHC will improve this measurement by a factor of about two. A one year dedicated run of the Linear

Collider at the threshold for $e^+e^- \rightarrow W^+W^-$ at 161 GeV might improve the mass error by another factor of two³⁴. Clearly, nothing much else goes on at that particular energy and the measurement would be tedious. It might eventually be worthwhile, if preceding measurements indicate a problem in this sector.

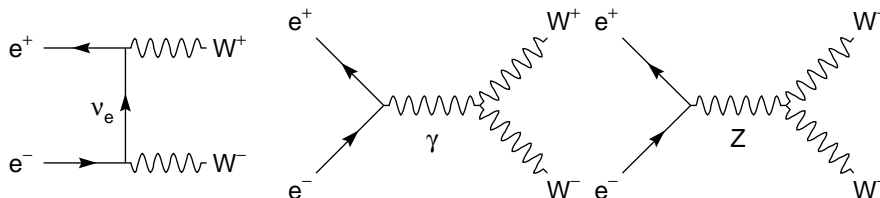


Figure 11. Born level Feynman graphs contributing to $e^+e^- \rightarrow W^+W^-$.

What will dramatically improve with a Linear Collider is the measurement of weak boson self couplings. These couplings define the electromagnetic and weak coupling constants via the γW^+W^- and ZW^+W^- vertices. They are measured using the reaction $e^+e^- \rightarrow W^+W^-$, as shown in Fig. 11. The measurement would proceed in much the same way as at LEP now, using the total cross section, the production angle and the decay angle distributions¹. Should deviations in these couplings be observed, they can be understood in terms of an effective Lagrangian³⁶ (imposing C and P invariance for simplicity)

$$\frac{i\mathcal{L}_{\text{eff}}}{g_{VWW}} = g_1^V V^\mu (W_{\mu\nu}^- W^{+\nu} - W_{\mu\nu}^+ W^{-\nu}) \quad (10)$$

$$\kappa_V W_\mu^+ W_\nu^- V^{\mu\nu} + \frac{\lambda_V}{M_W^2} V^{\mu\nu} W_\nu^{+\rho} W_{\rho\mu}^- \quad (11)$$

where the index $V = \gamma, Z$ identifies the neutral boson, V^μ and W^μ are the neutral and charged boson fields and $V^{\mu\nu}$ and $W^{\mu\nu}$ are their field tensors. The Lagrangian is normalised such that $g_{\gamma WW} = -e$ and $g_{ZWW} = -e \cot \theta_W$, so that the couplings $\kappa_V = 1$, $g_1^V = 1$ and $\lambda_V = 0$ reproduce the Standard Model trilinear couplings. The photonic couplings relate to the static properties of the W boson, like its charge, $q_W = eg_1^\gamma$, its magnetic dipole moment

$$\mu_W = \frac{e}{2M_W} (g_1^\gamma + \kappa_\gamma + \lambda_\gamma) \quad (12)$$

and its electric quadrupole moment

$$Q_W = -\frac{e}{M_W^2} (\kappa_\gamma - \lambda_\gamma). \quad (13)$$

Electromagnetic gauge invariance requires $g_1^\gamma = 1$. $SU(2)\times U(1)$ gauge invariance requires that deviations of the couplings from their standard values respect the relations

$$\Delta\kappa_Z = \Delta g_1^Z - \Delta\kappa_\gamma \tan^2 \theta_W \quad (14)$$

$$\lambda_Z = \lambda_\gamma \quad (15)$$

This way, the full wealth of fourteen anomalous trilinear couplings in the most general Lagrangian is reduced to only three: g_1^Z , $\Delta\kappa_\gamma$ and λ_γ . The existence of trilinear boson couplings is clearly established at LEP-200 and anomalous couplings are limited to a few percent¹.

At high energies, $\sqrt{s} - 2M_W \gg \Gamma_W$, the structure of the Lagrangian is the same for its γW^+W^- and ZW^+W^- components. Should anomalous couplings occur, it would thus be difficult to determine whether they are of electromagnetic or weak origin. The two contributions can however be disentangled with polarised beams, since the electromagnetic coupling is symmetric under $e_L \leftrightarrow e_R$, while the weak coupling is asymmetric. In addition, the so-called single W production reaction, $e^+e^- \rightarrow e^-W^+\bar{\nu}_e$, which is dominated by t -channel γW fusion, singles out the γW^+W^- vertex. At $\sqrt{s} = 500$ GeV, with an average electron polarisation of 80% on unpolarised positrons, and using a luminosity of 500 fb^{-1} , one can estimate the sensitivities³⁵ to anomalous couplings as summarised in Tab. 2. An improvement of several orders of magnitude is achieved with respect to present knowledge. At even higher energy, $\sqrt{s} \simeq 1$ TeV, these results would even be 20 to 50% better.

Table 2. Statistical sensitivity to anomalous couplings expected from a collider run at $\sqrt{s} = 500$ GeV, with an average electron polarisation of 80%, unpolarised positrons, and using a luminosity of 500 fb^{-1} .

Parameter	Statistical Error [$\times 10^{-3}$]
$\Delta\kappa_\gamma$	0.48
λ_γ	0.72
Δg_1^Z	2.50
$\Delta\kappa_Z$	0.79
λ_Z	0.65

Initial state polarisation can also be used to suppress large parts of the W pair production cross section, if it is a background to other studies. This is demonstrated in Fig. 12, where the unpolarised cross section is compared to cross sections with realistic electron beam polarisations as well as electron and positron beam polarisations.

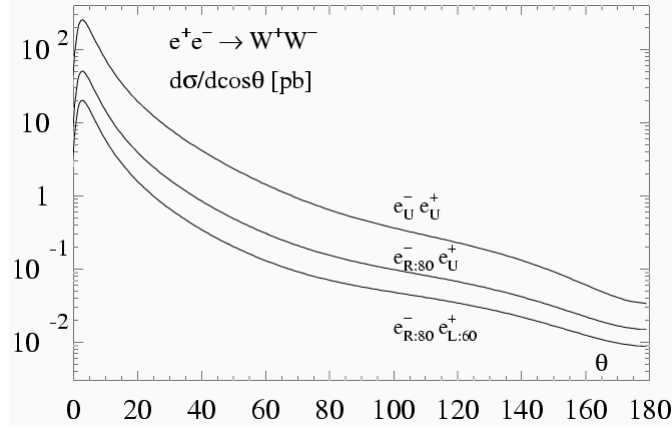


Figure 12. Born level differential cross section for $e^+e^- \rightarrow W^+W^-$. The unpolarised cross section is compared to the cross section with 80% electron beam polarisations as well as 80% electron and 60% positron beam polarisations.

6 Higgs Physics

The Higgs boson, if it exists in either its Standard Model form or in one of its supersymmetric variants, will be discovered at LHC. The study of its properties is one of the strong arguments in favour of a first generation Linear Collider. The production cross section for the Standard Model Higgs boson is large, as shown in Fig. 13. For modest Higgs boson masses, the production is dominated by boson fusion processes in $e^+e^- \rightarrow H e^+e^-$ and $e^+e^- \rightarrow H \nu \bar{\nu}$ final states. The contribution of the Higgsstrahlung process $e^+e^- \rightarrow HZ$, which has a sharper threshold, can be enhanced relative to boson fusion by initial state polarisation.

The Higgs decay properties are completely defined once its mass, M_H , is known. Above the respective thresholds, one has

$$\Gamma(H \rightarrow f\bar{f}) = \frac{G_F N_C}{4\sqrt{2}\pi} M_f^2 (M_H^2) M_H \quad (16)$$

$$\Gamma(H \rightarrow VV) = N_V \frac{\sqrt{2}G_F}{32\pi} M_H \quad (17)$$

with the Fermi constant G_F , the number of fermion colours N_C , the constant $N_V = 1, 2$ for $V = Z, W$ and the fermion and boson masses M_f and M_V . The Higgs boson is thus a narrow state unless it is so heavy that it can decay into

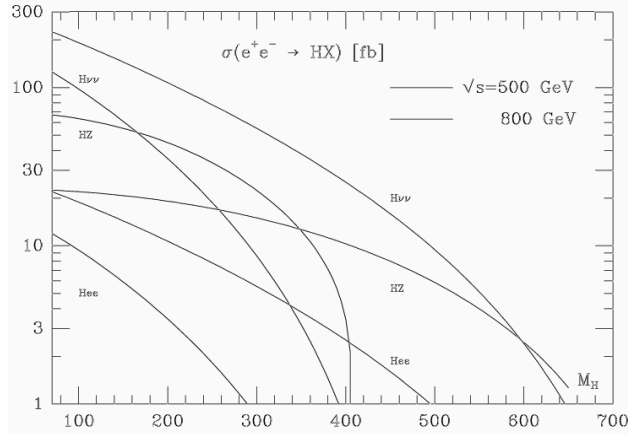


Figure 13. Higgs production cross section in the Standard Model as a function of the Higgs boson mass, at $\sqrt{s} = 500$ GeV (solid lines) and 800 GeV (dashed lines), separate for the Higgsstrahlung process and the WW and ZZ fusion processes.

W or Z bosons. This is demonstrated in Fig. 14, which shows the branching fractions and the total width as a function of the mass, for the Standard Model Higgs boson.

A prime task for the Linear Collider will be to precisely measure the Higgs boson mass. A determination of the threshold position gives best results³⁷. The mass error can be estimated as

$$\Delta M_H = \sqrt{\sigma_{ZH}} \left| \frac{\partial M_H}{\partial \sigma_{ZH}} \right| \frac{1}{\sqrt{\epsilon P \mathcal{L}}} \quad (18)$$

where σ_{ZH} is the Higgsstrahlung cross section, $\partial M_H / \partial \sigma_{ZH}$ is the inverse of the cross section's sensitivity to mass, ϵ the experimental selection efficiency for Higgs events, P the average electron polarisation and \mathcal{L} the integrated luminosity. As an example, for a narrow Higgs of $M_H = 120$ GeV and $\mathcal{L} = 130$ fb⁻¹, one would have $\Delta M_H = 30 \text{ MeV} / \sqrt{\epsilon P}$. For a wider one of $M_H = 180$ GeV and $\mathcal{L} = 170$ fb⁻¹, the error would still be $\Delta M_H = 60 \text{ MeV} / \sqrt{\epsilon P}$. With all Higgs decay channels observed, one can hope for $\epsilon P \simeq 0.5$, and thus a mass error of 50 to 100 MeV depending on the mass, as well as a Higgs width measurement with of order 10% accuracy.

The Higgs boson decay properties should establish that it indeed supplies the functionality it has in the Standard Model, i.e. that it generates the masses of all fermions and vector bosons. To verify that, one needs to measure its

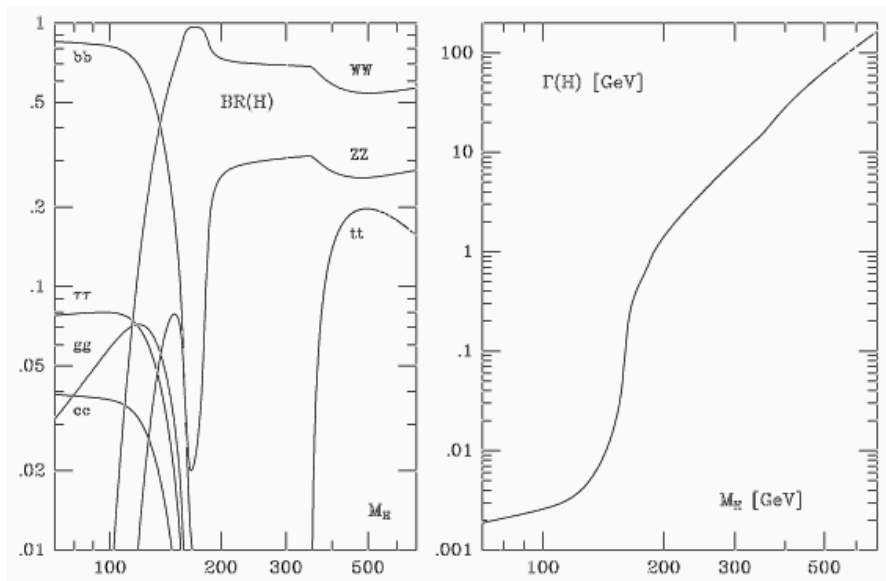


Figure 14. Higgs decay branching fractions (left) and total Higgs decay width (right) as a function of the Higgs boson mass in the Standard Model.

couplings to all these particles and compare them to the prediction. It does not suffice to cover only the dominant decay modes. In a very complete simulation study, Battaglia³⁸ has shown that it is indeed possible to tag the majority of Higgs decays using topological as well as secondary vertex tags fed into a neutral network. Decays into b and c as well as light quarks can thus be separated from each other. This way, the decay branching fractions for $H \rightarrow b\bar{b}$, $c\bar{c}$, $\tau^+\tau^-$, gluon and W pairs can be measured as shown in Fig 15. Using 100 fb^{-1} of luminosity at 350 to 500 GeV center of mass energy and for a Higgs boson mass between 110 and 140 GeV, one expects accuracies that vary between 5% for $b\bar{b}$ and 8% for $c\bar{c}$.

To judge this accuracy, a good way is to gauge it against close alternatives to the Standard Model Higgs boson, like the lightest Higgs boson, h^0 , in minimal supersymmetry (MSSM). The MSSM decay widths are approximately related to the Standard Model ones by the supersymmetry parameters α and

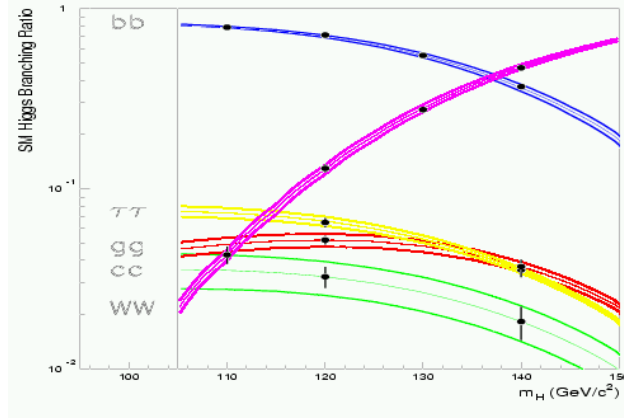


Figure 15. Measurement of the Higgs decay branching fractions into fermion and boson pairs.

β such that

$$\Gamma_{b\bar{b}}^{\text{MSSM}} \sim \Gamma_{b\bar{b}}^{\text{SM}} \frac{\sin^2 \alpha}{\cos^2 \beta} \quad (19)$$

$$\Gamma_{c\bar{c}}^{\text{MSSM}} \sim \Gamma_{c\bar{c}}^{\text{SM}} \frac{\cos^2 \alpha}{\sin^2 \beta} \quad (20)$$

$$\Gamma_{WW^*}^{\text{MSSM}} \sim \Gamma_{WW^*}^{\text{SM}} \quad (21)$$

The parameter $\tan \beta$ is the ratio of the vacuum expectation values for the two Higgs boson doublets required in the MSSM. The other angle is defined by $\tan \alpha = (M_Z^2 - M_A^2) \sin \beta \cos \beta / (M_H^2 - M_Z^2 \cos^2 \beta - M_A^2 \sin^2 \beta)$. With the branching ratio measurements alone one is thus able to distinguish between the Standard Model Higgs boson and the lightest member of the MSSM two doublet alternative in a large region of the MSSM parameter space, as shown in Fig. 16.

In addition to neutral Higgs bosons, supersymmetry requires the existence of charged Higgs bosons, H^\pm . These are copiously produced in e^+e^- annihilation and decay into fermion pairs like $\tau\nu$, $b\bar{t}$ and $s\bar{c}$, or boson pairs like hW or AW . These decays are characteristic enough to be selected with low backgrounds⁹, and accurate mass measurements from the production threshold position can be envisaged.

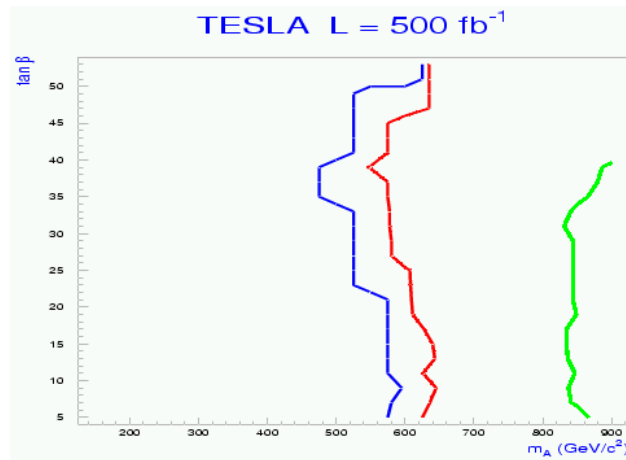


Figure 16. Regions in the M_A - $\tan\beta$ plane, where the MSSM is distinguishable from the Standard Model, given the Higgs branching fractions measured at a Linear Collider. The lines correspond to 68%, 90% and 95% confidence level from right to left, with the distinguishable regions to the left of the lines.

7 Supersymmetric Particles

Many theoretical arguments make it attractive to restore symmetry between matter made of fermions and forces transmitted by vector bosons, by introducing supersymmetry³⁹. It stabilises radiative corrections by cancellation between fermionic and bosonic loops⁴⁰. It may also allow a grand unification of forces by introducing intermediate scales between the electroweak and the GUT scale⁴¹. However, introducing supersymmetry also opens Pandora's box in that both the particle spectrum and the number of parameters in the theory expand considerably. To make supersymmetric models at all predictive, additional assumptions are necessary even for its minimal implementations. Popular models are based on minimal supergravity⁴² (mSUGRA) or gauge mediated supersymmetry breaking⁴³ (GMSB). Both models have been studied extensively for the Linear Collider^{44,45}.

What really matters at a Linear Collider is less the discovery of supersymmetric states. Although a few of them like charginos and neutralinos are hard to produce at a hadron collider, one can assume that a fair fraction of the supersymmetric spectrum will have been observed at the LHC. As an example, Fig. 17 shows a plausible spectrum of particles and decay modes as expected

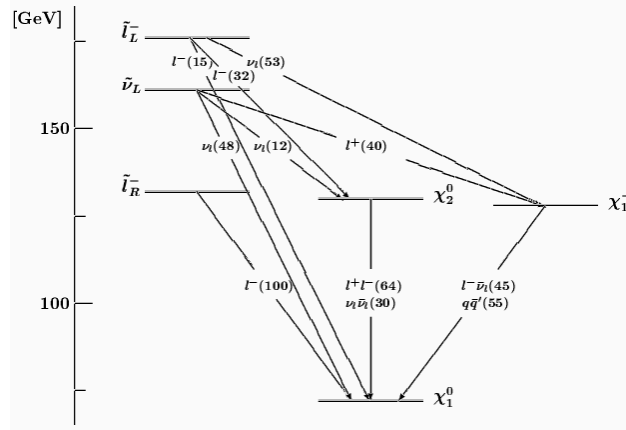


Figure 17. Mass spectrum and decay modes of sleptons and light gauginos in a mSUGRA scenario.

in mSUGRA models. The rôle of the Linear Collider will be to complete this spectrum and precisely determine masses and couplings. All this in order to tell which kind of supersymmetry is realised in nature, by a determination of its (many) parameters.

The chargino and neutralino production thresholds are fairly marked even when ISR and beamstrahlung are taken into account. Fig. 18 shows the production cross section and dijet invariant mass distributions for a chargino mass of 170 GeV, at $\sqrt{s} \simeq 500$ GeV. One concludes that the mass of the lightest chargino can be measured with about 200 MeV accuracy from the continuum production and 40 MeV from a threshold scan⁴⁴. Similar results are obtained for neutralinos.

The threshold for sleptons is smoother and the mass determination less accurate as can be seen in Fig. 19. Nevertheless the simultaneous study of threshold cross section and continuum decay spectrum will allow the determination of slepton masses with a few hundred MeV accuracy⁴⁴.

These measurements can then be used in a RGE analysis of the mass spectrum to determine the underlying SUSY model and its parameters. Taking a mSUGRA scenario as a guideline example, one would thus expect to measure the supersymmetry parameters with a respectable accuracy⁴⁴, as indicated in Tab. 3. Polarisation of electrons and positrons is very important for such a study since it allows to suppress dominant backgrounds.

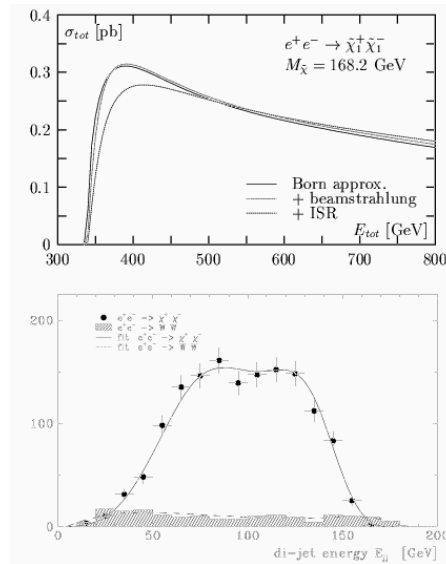


Figure 18. Top: Production cross section for chargino pairs of 168.2 GeV mass as a function of center of mass energy. Bottom: Dijet energy spectrum in continuum chargino decays at center of mass energies around 500 GeV.

Table 3. Accuracy of supersymmetry parameters determined from the accessible mass spectrum of sleptons and light gauginos at a Linear Collider. As an example, parameters from a mSUGRA scenario have been used.

Parameter	Assumed value	Expected error
m_0	100 GeV	0.09 GeV
M_1	200 GeV	0.20 GeV
M_2	200 GeV	0.20 GeV
A_0	0 GeV	10.3 GeV
$\tan \beta$	3.0	0.04
$sgn(\mu)$	+	fixed

8 Alternative New Physics

In case nature chose not to make use of the Higgs mechanism, something else must be responsible for particle masses. Candidates include extra dimensions⁴⁶, which might also be transmitting gravitational interactions⁴⁷. The mass of ordinary particles might thus be an artefact of just observing

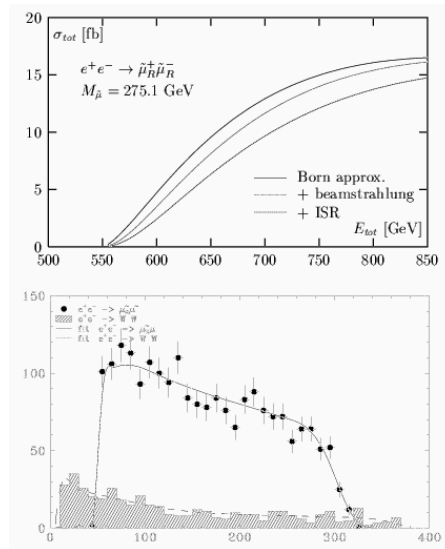


Figure 19. Top: Production cross section for smuon pairs of 275.1 GeV mass as a function of center of mass energy. Bottom: Muon energy spectrum in continuum smuon decays at center of mass energies around 800 GeV.

propagation in a subset of the existing dimensions, e.g. via so-called Kaluza-Klein towers. Gravitons might populate extra dimensions and gravity might be of geometric origin after all. Effects of this idea at a Linear Collider have been looked into⁴⁶. An example is given in Fig. 20, which shows the cross section for one of the signatures, single energetic photons, as a function of the fundamental mass scale M_D . The signal would be an order of magnitude above irreducible Standard Model background if the mass scale is not too large.

In the Standard Model, the Higgs particle also cancels divergences in boson couplings, like WW scattering. If it does not exist, additional strong inter-boson interactions might provide a cut off, instead. These would become apparent at a Linear Collider as vector or scalar resonances between W bosons in $e^+e^-W^+W^-$, $\nu\bar{\nu}W^+W^-$ and $\nu\bar{\nu}ZZ$ final states⁹, as shown in Fig. 21.

From the cross section measurements, the couplings of the new interactions are derived^{48,49}. As shown in Fig. 22, high luminosity measurements at a Linear Collider cover the whole WW threshold region and completely determine the relevant couplings. Very high luminosities, of order 1000 fb^{-1} ,

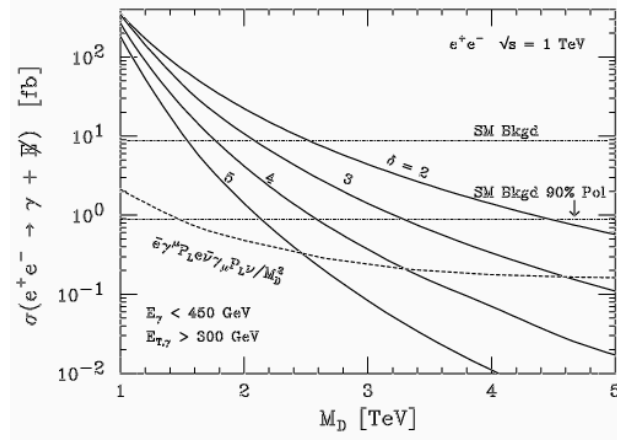


Figure 20. Total cross section for the reaction $e^+e^- \rightarrow \gamma + \cancel{E}$ at $\sqrt{s} = 1 \text{ TeV}$, as a function of the fundamental mass scale M_D . Solid lines are for graviton production with variable number of extra dimensions, δ . The dashed-dotted lines represent Standard Model background without and with 90% electron beam polarisation.

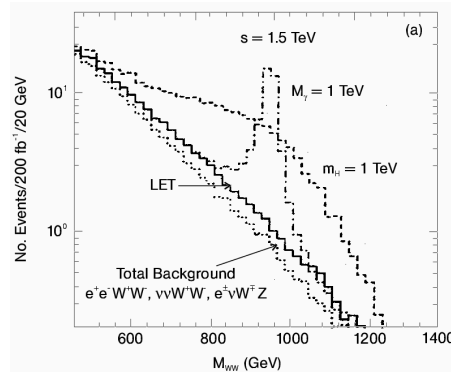


Figure 21. Mass distribution of WW pairs for vector and scalar resonances at a Linear Collider compared to Standard Model background.

and high beam polarisations are required for such a measurement.

Since neither baryon nor lepton number is protected by a gauge symmetry, nature might have states in stock that carry both quantum numbers. The production cross section for leptoquarks at a Linear Collider would be large,

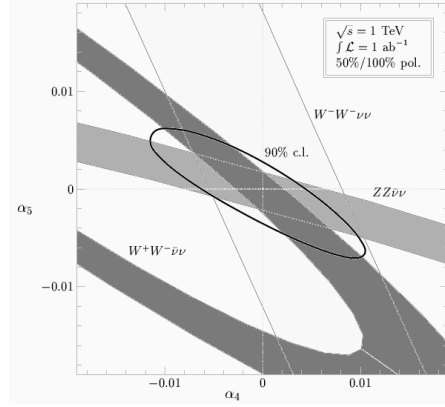


Figure 22. Allowed regions in the expansion parameters in chiral electroweak models from a cross section measurement for W^+W^- and ZZ production at very high luminosities and beam polarisations. Additional constraints might come from a measurement of $e^-e^- \rightarrow \nu\nu W^-W^-$.

between 10 and 1800 fb^{-1} depending on the leptoquarks charge, spin and other properties^{9,50}, as shown in Fig. 23. Thus, if worst comes to worst, leptoquark spectroscopy would be the *pièce de résistance* of experimentation at a Linear Collider.

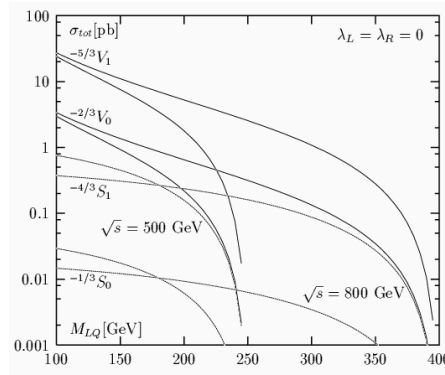


Figure 23. Total cross sections for scalar and vector leptoquark pair production, at $\sqrt{s} = 800 \text{ GeV}$, as a function of the leptoquark mass. Corrections due to beamstrahlung and ISR are included.

9 Conclusions and Outlook

Experiments at LEP have established the current effective theory, the Standard Model. In these lectures, I have tried to substantiate my view that there will be a sharing of responsibilities between LHC and a future electron-positron Linear Collider. Experimentation at LHC will cross the limits of validity of the Standard Model and outline a new effective theory to replace it. A Linear Collider, covering *grosso modo* the same energy range, is then needed to establish that next effective theory.

After almost 10 years of study, we can now be confident that the Tesla project has a machine design that is both feasible and fulfils the physics requirements for a first generation Linear Collider after LHC. An excellent detector for Tesla can be built with reasonable extrapolations of today's technologies.

Based on the Tesla Conceptual Design Report⁸, optimisation of machine and detector is progressing rapidly. A costed proposal will be published in the form of a Technical Design Report later in 2000 or early in 2001. This will be followed by an in depth discussion within the international particle physics community and with the funding bodies, in the context of similar proposals elsewhere. In a most optimistic scenario, if approved by 2003, first beams from Tesla could be seen by 2008, at the earliest.

Due to its built in limitations in center of mass energy, Tesla will be followed by machines exploiting energy ranges beyond LHC. A very promising contender would be a two beam accelerator like CLIC⁵¹, whose characteristics might look like the summary in Tab. 4, and for which physics studies have just started. Such a machine will clearly go beyond the regional scope of its predecessors. It will require a truly world-wide effort, for the development of its novel acceleration technologies and of the appropriate tools for experimentation. One might hope that accelerator laboratories would form a world wide network to support such a machine, following the example of experimental collaborations that have done the same for a long time already.

Acknowledgements

I would like to thank the organisers of this meeting, especially Prof. Manuel Aguilar Benitez, Dr. Isabel Josa Mutuberría and Dr. Juan Alcaraz, for their fabulous hospitality, rooted in the Spanish tradition. I would also like to thank all participants of the meeting for creating a stimulating atmosphere of exchange and discussion.

Table 4. Outlook to possible machine parameters at the CLIC two-beam collider project.

	CLIC	
type	Two Beam Linear Collider	
maximum energy	1000 GeV	3000 GeV
total length	10km	40km
accelerating gradient	150 MV/m	170 MV/m
maximum bunches	154	
beam size at IP [μm]	0.115×0.002	0.030×0.001
luminosity [$\text{cm}^{-2}\text{s}^{-1}$]	2×10^{34}	10×10^{34}

References

1. J. Mnich, *LEP-200 Physics*, XXVIII International Meeting on Fundamental Physics, Sanlúcar de Barrameda, Cádiz, Spain, 14-18 February 2000, these proceedings.
2. N. Cabibbo, *Phys. Rev. Lett.* **10**, 531 (1963).
3. M. Kobayashi and T. Maskawa, *Prog. Theor. Phys.* **49**, 652 (1973)
4. Z. Maki, M. Nakagawa and S. Sakata, *Prog. Theor. Phys.* **28**, 870 (1962)
5. C.M. Ankenbrandt *et al.* (Muon Collider Collab.), *Status of muon collider research and development and future plans*, *Phys. Rev. ST Accel. Beams* **1**, 081001 (1999).
6. See <http://www.desy.de/conferences/ecfa-desy-1c98.html>.
7. See <http://lcwss.physics.yale.edu/lc/>.
8. R. Brinkmann *et al.*, *Conceptual Design Report of a 500 GeV e^+e^- Linear Collider with Integrated X-ray Laser Facility*, DESY Report DESY 1997-048 (1997).
9. E. Accomando *et al.*, *Phys. Rept.* **299**, 1 (1998).
10. See <http://www.cern.ch/Physics/LCWS99/>.
11. See <http://ireswww.in2p3.fr/ires/ecfadesy/index.html>.
12. See <http://www-project.slac.stanford.edu/nlc/home.html>.
13. See <http://www-jlc.kek.jp/>.
14. R. Brinkmann, *High Luminosity with TESLA-500*, DESY Report TESLA 97-13 (1997).
15. F. Kircher *et al.*, *Status report on the CMS superconducting solenoid for LHC*, DAPNIA-STCM-98-11 (1998).
16. See e.g. A.C. Benvenuti *et al.*, *Nucl. Instrum. Methods* **A290**, 353 (1990).
17. E. Heyne and P. Jarron, *Nucl. Instrum. Methods* **A275**, 467 (1989).
18. C.J.S. Damerell, *Nucl. Instrum. Methods* **A342**, 78 (1994).
19. K.H. Becks *et al.*, *Nucl. Instrum. Methods* **A386**, 11 (1997).
20. M. Caccia *et al.*, *High resolution pixel detectors for e^+e^- Linear Collid-*

- ers, 4th International Workshop on Linear Colliders (LCWS 99), Sitges, Barcelona, Spain, 28 April - 5 May 1999, hep-ex/9910019.
21. D. Decamp *et al.*, *Nucl. Instrum. Methods* **A294**, 121 (1990).
 22. D. Buskulic *et al.*, *Nucl. Instrum. Methods* **A360**, 481 (1995).
 23. F. Sauli, *Nucl. Instrum. Methods* **A386**, 531 (1997).
 24. A. Benvenuti *et al.*, *STIC, the new Delphi Luminosity Monitor*, 4th International Conference on Calorimetry in High-Energy Physics, La Biodola, Italy, 19-25 Sep. 1993, p. 165.
 25. E. Hartouni *et al.* (HERA-B Collab.), HERA-B Design Report, DESY-PRC 95/01 (1995).
 26. See e.g. A. Henriques *et al.* (TILECAL Collab.), *The Atlas Tile Calorimeter Project*, 4th International Conference on Advanced Technology and Particle Physics, Como, Italy, 3-7 Oct. 1994, *Nucl. Phys. Proc. Suppl.* **44**, 82 (1995).
 27. B.E. Anderson *et al.* (OPAL Collab.), *IEEE Trans. Nucl. Sci.* **41**, 845 (1994)
 28. D. Bederede *et al.* (ALEPH Collab.), *Nucl. Instrum. Methods* **A365**, 117 (1995).
 29. H. Videau, *Calorimeter Design*, 2nd ECFA/DESY Study on Physics and Detectors for a Linear Electron-Positron Collider, Obernai, France, 16-19 Oct. 1999.
 30. J.C. Brient, *SiW Calorimeter Performance*, 2nd ECFA/DESY Study on Physics and Detectors for a Linear Electron-Positron Collider, Obernai, France, 16-19 Oct. 1999.
 31. M. Pohl and H.J. Schreiber, *SIMDET - Version 3, A Parametric Monte Carlo for a Tesla Detector*, DESY Report 99-030 (1999).
 32. P. Comas *et al.*, *The physics of the $e^+e^- \rightarrow t\bar{t}$ threshold scan*, CERN-PPE/96-40 (1996) and DESY 96-123D (1996).
 33. G.P. Zeller *et al.*, *A measurement of $\sin^2 \theta_W$ in νN scattering from NuTeV*, Proceedings of American Physical Society (APS) Meeting of the Division of Particles and Fields (DPF 99), Los Angeles, CA, 5-9 Jan. 1999, and hep-ex/9906024.
 34. T. Ohl, *Electroweak Physics*, 2nd ECFA/DESY Study on Physics and Detectors for a Linear Electron-Positron Collider, Obernai, France, 16-19 Oct. 1999.
 35. K. Mönig, *Beam Polarisation for Electroweak Physics*, 2nd ECFA/DESY Study on Physics and Detectors for a Linear Electron-Positron Collider, Obernai, France, 16-19 Oct. 1999.
 36. K. Hagiwara *et al.*, *Nucl. Phys.* **B282**, 253 (1987).
 37. G.W. Wilson and K. Desch, *Measuring M_H Using $e^+e^- \rightarrow ZH$ at Thresh-*

- old*, 2nd ECFA/DESY Study on Physics and Detectors for a Linear Electron-Positron Collider, Obernai, France, 16-19 Oct. 1999.
38. M. Battaglia, *Measuring Higgs Branching Ratios and Telling the SM from a MSSM Higgs Boson at the e^+e^- Linear Collider*, 4th International Workshop on Linear Colliders (LCWS 99), Sitges, Barcelona, Spain, 28 April - 5 May 1999, University of Helsinki Report HU-P-264 (1999), hep-ph/9910271.
 39. J. Wess and B. Zumino, *Nucl. Phys.* **B70**, 39 (1974).
 40. See e.g. M. Drees, *An Introduction to Supersymmetry*, Lectures given at Inauguration Conference of the Asia Pacific Center for Theoretical Physics (APCTP), Seoul, Korea, 4-19 June 1996, hep-ph/9611409
 41. U. Amaldi *et al.*, *Phys. Rev.* **D36**, 1385 (1987).
 42. A.P. Nilles, *Phys. Rept.* **110**, 1 (1984).
 43. G.F. Giudice and R. Rattazzi, *Phys. Rept.* **322** 419 (1999), and *Phys. Rept.* **322**, 501 (1999).
 44. H.U. Martyn and G.A. Blair, *Determination of Sparticle Masses and SUSY Parameters*, 4th International Workshop on Linear Colliders (LCWS 99), Sitges, Barcelona, Spain, 28 April - 5 May 1999, hep-ph/9910416.
 45. S. Ambrosanio and G.A. Blair, *Precision GMSB at a Linear Collider*, 4th International Workshop on Linear Colliders (LCWS 99), Sitges, Barcelona, Spain, 28 April - 5 May 1999, hep-ph/9907396.
 46. G.F. Giudice, R. Rattazzi and J.D. Wells, *Nucl. Phys.* **B544**, 3 (1999).
 47. N. Arkani-Hamed, S. Dimopoulos and G. Dvali, *Phys. Lett.* **B429**, 263 (1999).
 48. E. Boos *et al.*, *Phys. Rev.* **D57**, 1553 (1998).
 49. E. Boos *et al.*, *Phys. Rev.* **D61**, 077901 (2000).
 50. M. Heyssler, R. Rückl and H. Spiessberger, *Leptoquark and R-Parity Violating SUSY Processes*, 4th International Workshop on Linear Colliders (LCWS 99), Sitges, Barcelona, Spain, 28 April - 5 May 1999, hep-ph/9908319.
 51. See <http://clicphysics.web.cern.ch/CLICphysics/>.